

# Realization of a narrow-band filter for methane gas detection

FU XIU-HUA<sup>a</sup>, CHEN CHENG<sup>a,\*</sup>, XIONG SHI-FU<sup>a,b,\*</sup>, ZHANG JING<sup>a</sup>

<sup>a</sup>*School of Photo-Electronic Engineering, Changchun University of Science and Technology, Changchun 130022, China;*

<sup>b</sup>*Institute of Functional Crystals, Tianjin University of Technology, Tianjin 300384, China*

Natural gas leaks frequently during exploitation, transportation, storage and use. It can cause energy loss and even cause fire, explosion and other consequences, seriously threaten people's lives and property. Methane is the main component of natural gas, and its effective detection and identification is of great significance for timely detection of natural gas leakage accidents. Various approaches have been proposed to detect methane, however the detection and identification of methane leakage by infrared technology has become a hot topic in the world. A narrow-band filter developed based on the infrared characteristic absorption peak of methane is one of the core optical components of the detection system. At present, Narrow-band filter for methane infrared imaging system has low peak transmittance and narrow cut-off area. The sensitivity of the system can be improved by increasing the peak transmittance and widening the cut-off area. In this paper, the design of the filter is achieved by using the principle of splitting technique. By analyzing the sensitivity of the membrane layer and adjusting the monitoring mode of the membrane layer, the thickness of the sensitive layer can be controlled accurately. The peak transmittance of the filter reached 87.88% at the wavelength of 7.669 $\mu\text{m}$ , the full width of its passband at half maximum is 71nm, which better suppresses the background noise and improves the sensitivity of the detection system.

(Received February 16, 2019; accepted October 9, 2019)

*Keywords:* Optical thin film, Narrow-band filter, Monitoring mode, Gas leaks, Sensitivity

## 1. Introduction

On June 23, 2018, Science published the latest research report of the US Methane Leakage Research led by the US Environmental Protection Agency [1]. The New York Times quoted the report as saying that the US oil and gas industry's methane leakage accounted for 2.3% of total annual production, 60% higher than the Environmental Protection Agency's estimate of 1.4%.

Methane is the main component of natural gas. Methane's leaks will bring two problems: on the one hand, it not only causes energy loss, but even causes major disasters such as fires and explosions [2,3]. Accidents are a serious threat to people's lives, property, social harmony and stability. On the other hand, methane is a strong greenhouse gas. According to the data, the global warming potential of methane is 72 times that of carbon dioxide (20-year ago). Methane emission reduction has an important foundation in the national climate change strategy [4]. Therefore, the realization of the identification and detection of methane gas can effectively reduce the impact of methane gas leakage.

Passive infrared thermal imaging detection technology based on background radiation absorption has been widely used in the field of gas detection [5]. As one

of the core optical components of gas detection and identification system, infrared filter plays an important role in the accuracy of the detection system. In 2017, ShiFu Xiong et al. developed narrow-band pass filter components for infrared thermal imager. The peak transmittance of the filter reached 85.14% at the wavelength of 7.669 $\mu\text{m}$ , the full width of its passband at half maximum is 59nm, and the cut-off area is 6~7.5 $\mu\text{m}$  and 7.8~14 $\mu\text{m}$  [6]. In 2018, P. Wang et al. [7] developed a narrow-band filter with a center wavelength of 3.33  $\mu\text{m}$ , with BPF bandwidths of 160 nm and 300 nm. The BPF spectral stability for various environmental temperature and humidity conditions is demonstrated. On this basis, the peak transmittance is further improved, and widening the cut-off area is very important for improving the resolution and sensitivity of the passive methane infrared thermal imaging detection system.

## 2. Structure design of the filter

The schematic diagram of the methane gas detection and identification system is shown in Fig. 1. It consists of an optical imaging system, a narrow-band filtering system and a signal processing output system.

The optical imaging system consists primarily of an infrared lens and a lens interface. Its main function is to collect and focus the infrared radiation signals of the gas and the background onto the imaging surface, that is, the uncooled infrared focal plane detector. The narrow-band filtering system is mainly composed of an infrared filter and a coding motor. The encoder motor in turn rotates the filter to a focal plane detector and filters the radiation signal collected by the optical imaging system.

The signal processing output system is mainly

composed of an infrared focal plane detector, a processing circuit, an analysis processing unit, and a display alarm output module. The analysis processing unit is a data processing center of the detection system, and analyzes the infrared radiation signal received by the detector. Processing, identifying the detected gas, and transmitting the image and processing results to the display output module. The display and alarm output modules provide corresponding display and alarm responses to system processing results.

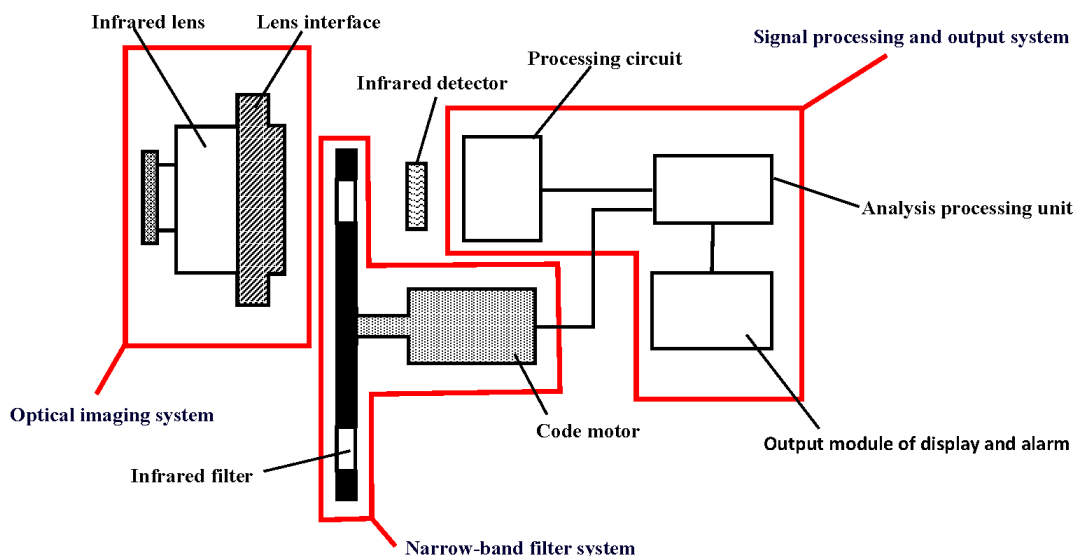


Fig. 1. Schematic diagram of detection and identification system of  $CH_4$

The performance parameters of the filter are determined by the characteristic absorption peak of methane gas in the atmosphere. From the HITRAN database, it is found that there are four characteristic absorption peaks of methane molecules in the infrared region [8]. As shown in Fig. 2, the absorption peak in the near-infrared region is at a wavenumber of  $6250\text{ cm}^{-1}$  (corresponding to a wavelength of  $1.6\ \mu\text{m}$ ) and a wavenumber of  $4348\text{ cm}^{-1}$  (corresponding to a wavelength of  $2.3\ \mu\text{m}$ ), which of the absorption peaks are weak. While in the mid-infrared characteristic absorption, there are two strong absorption peaks at the peak of  $3021\text{ cm}^{-1}$  (corresponding to the wavelength of  $3.31\ \mu\text{m}$ ) and the far-infrared characteristic absorption peak of  $1303\text{ cm}^{-1}$  (corresponding wavelength is  $7.669\ \mu\text{m}$ ).

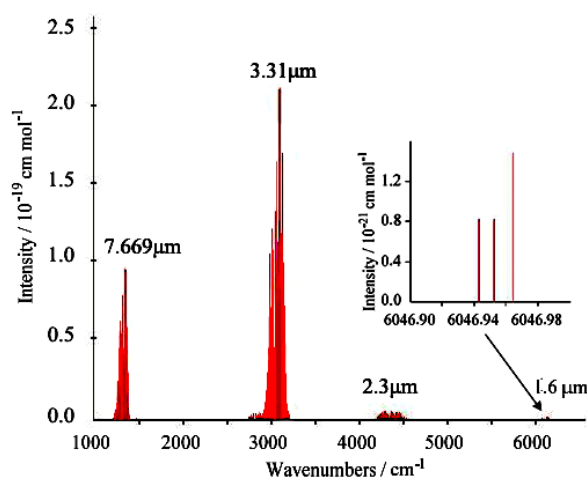


Fig. 2. Characteristic absorption peak of methane gas in atmosphere

Since the selected detector is a Pico640ETM uncooled focal plane detector module produced by ULIS, France, the spectral response range is  $3\sim 14\ \mu\text{m}$ , so the

absorption peaks of  $1.6\mu\text{m}$  and  $2.3\mu\text{m}$  are not considered, and the absorption intensity of  $3.31\mu\text{m}$  is twice more than  $7.669\mu\text{m}$ , which is the ideal band for gas detection. However, the absorption peaks of most organic substances such as alkanes, alkenes and alkynes are between  $3.2$  and  $3.4\mu\text{m}$ , so they can also be detected. The presence of gas is unrecognizable, that is, it is uncertain whether the detected gas is methane. At  $7.669\mu\text{m}$ , there is a strong absorption peak, and also no obvious absorption peak of other organic gases in this band, although the water vapor absorption does have an effect on the detection of methane. However, as early as 2012, Shanwen Sun et al. [9] studied the effect of water concentration on methane detection performance. The results show that the detection and identification of methane gas can be achieved in a certain range of water vapor concentration. Considering comprehensively, it is advisable to use the characteristic absorption peak at  $7.669\mu\text{m}$  to detect and identify methane.

The optical performance parameters of the narrow-band filter of the methane gas infrared thermal imaging system are determined by the characteristic absorption peak of methane at the characteristic absorption wavelength of  $7.669\mu\text{m}$  of the selected methane gas [10]. The narrow-band filter should have accurate wavelength localization, high peak transmittance, and good background stray light suppression.

This paper uses a foundation of a full-media Fabry-Perot filter [11], as shown in Fig. 3, reflective films on both sides of the resonator are represented by equivalent interfaces a and b.

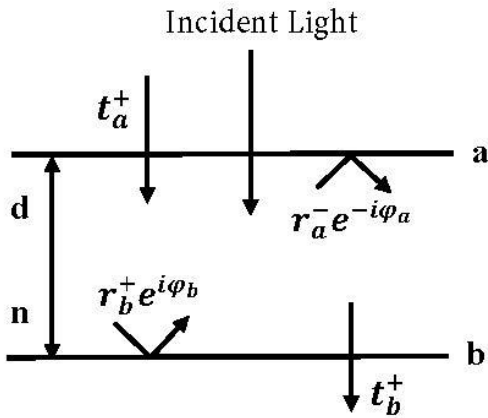


Fig. 3. Equivalent interface structure of F-P bandpass filter

The reflection coefficients and transmission coefficients of the a and b interfaces are denoted as  $r_a^- e^{-i\varphi_a}$ ,  $r_b^+ e^{i\varphi_b}$ ,  $t_a^+$ ,  $t_b^+$  respectively. Where  $\varphi_a$  and  $\varphi_b$  represent the phase difference between the light

before and after reflection at the interface a, b. The transmission coefficient of the filter is,

$$t = \frac{t_a^+ t_b^+}{1 - |r_a^-| |r_b^+| e^{i(\varphi_a + \varphi_b - 2\delta)}} \quad (1)$$

where  $\delta = 2\pi n d / \lambda$ ,  $n$  represents the refractive index of the film, and  $d$  represents the physical thickness of the film. In the case where the matching medium on both sides of the filter is the same, the transmittance is

$$T = \frac{|t_a^+|^2 |t_b^+|^2}{(1 - |r_a^-| |r_b^+|)^2 \left[ 1 + \frac{4|r_a^-| |r_b^+|}{(1 - |r_a^-| |r_b^+|)^2} \sin^2 \frac{1}{2}(\varphi_a + \varphi_b - 2\delta) \right]} \quad (2)$$

$$T_a = |t_a^+|^2 \quad T_b = |t_b^+|^2 \quad R_a = |r_a^-|^2 \quad R_b = |r_b^+|^2 \quad (3)$$

$$\text{Let } R = \sqrt{R_a R_b} \quad T_s = \frac{T_a T_b}{(1 - R)^2} \quad F = \frac{4R}{(1 - R)^2}$$

$$\theta = \frac{1}{2}(\varphi_a + \varphi_b - 2\delta)$$

The transmittance of the filter is

$$T(\lambda) = \frac{T_s}{1 + F \sin^2 \theta} \quad (4)$$

The  $\text{CH}_4$  characteristic absorption spectrum is represented by the function  $f(\lambda)$ , and the spectral response sensitivity of the infrared detector Pico640E<sup>TM</sup> is expressed by the function  $C(\lambda)$ , then the response sensitivity  $P(\Delta\lambda)$  of the system can be expressed as

$$P(\Delta\lambda) = \frac{\int_{\lambda_0 - \Delta\lambda}^{\lambda_0 + \Delta\lambda} C(\lambda) \cdot T(\lambda) \cdot f(\lambda) d\lambda}{\int_{\lambda_0 - \Delta\lambda}^{\lambda_0 + \Delta\lambda} C(\lambda) \cdot T(\lambda) d\lambda} \quad (5)$$

It can be seen from formula (5) that the response sensitivity of the system is related to the transmittance and absorption spectral function of the filter. Due to the fact that  $T(\lambda)$  is a large value in a very small passbandrange  $(\lambda_0 - \Delta\lambda, \lambda_0 + \Delta\lambda)$  near the central wavelength, while in the other bands is basically zero. Thus, the detector response sensitivity  $C_0$  can be considered as a constant in a very small passband range  $(\lambda_0 - \Delta\lambda, \lambda_0 + \Delta\lambda)$ , The formula (5) simplifies to

$$P(\Delta\lambda) = \frac{\int_{\lambda_0 - \Delta\lambda}^{\lambda_0 + \Delta\lambda} T(\lambda) \cdot f(\lambda) d\lambda}{\int_{\lambda_0 - \Delta\lambda}^{\lambda_0 + \Delta\lambda} T(\lambda) d\lambda} \quad (6)$$

The difficulty coefficient  $Q(\Delta\lambda_0)$  for the preparation of narrow-band filters is closely related to its center wavelength  $\lambda_0$  and peak half-width  $2\lambda_0$ . With the peak half-width reduction, the difficulty increases sharply, and the higher the difficulty coefficient of preparation is, the higher the development costs. For simplicity, it can be described by exponential function model according to experience

$$Q(\Delta\lambda) = e^{\frac{\alpha(\lambda_0)}{2\Delta\lambda}} \quad (7)$$

In the formula (7),  $\alpha(\lambda_0)$  is an amount related to the control precision of the vacuum coating apparatus and the center wavelength  $\lambda_0$ . In practical engineering applications, both high sensitivity and low development cost are required. There is a certain contradiction between the two. Therefore, it is necessary to find an optimal compromise point, that is the cost-performance function, which is the ratio of the response sensitivity of the system to the difficulty of preparation. Assuming  $S(\Delta\lambda)$  is a cost-performance function, it can be

denoted as:

$$S(\Delta\lambda) = \frac{P(\Delta\lambda)}{Q(\Delta\lambda)} \quad (8)$$

Theoretically, there should be a half-width to maximize the cost-performance evaluation function. However, in actual engineering applications, whether the cost-effective index can be achieved depends on the control accuracy of the equipment. When the cost performance evaluation function reaches the maximum value, the half-width does not exceed the expected control precision of the device, and the half-width value can be appropriately reduced until the limit index is reached. At this time, the value of the cost performance function is not the maximum, but the detection system will obtain higher sensitivity.

The bandwidth of narrow-band filter is estimated by analyzing the evaluation function and combining with the control precision of actual equipment, and the specific technical parameters of narrow-band filter are obtained, the technical parameters are shown in Table 1.

Table 1 Technical parameter

Parameter	Specification
Center wavelength/ $\mu\text{m}$	7.669
Incident angle/ $^\circ$	0
Half width of passband/ $\mu\text{m}$	0.07
Peak transmittance/%	>85
Cut-off region/ $\mu\text{m}$	3~7.5 and
Transmittance of the cut-off	$\leq 0.5$

### 3. Material selection

When selecting materials, it is necessary to consider the transparency, refractive index, extinction coefficient, mechanical firmness and chemical stability of materials, but also to pay attention to the matching between film materials and the preparation process conditions. The spectral transmission region of narrow-band filter with the central wavelength of 7.669 $\mu\text{m}$  belongs to the LWIR band. The coating material was considered synthetically

in the LWIR band, Ge was chosen as a high refractive index material, and its transparent region is 1.7~23 $\mu\text{m}$ , and it has excellent mechanical fastness and chemical stability. The residual stress of Ge film is tensile stress when prepared by electron beam evaporation. The middle refractive index materials are generally selected from ZnSe and ZnS, however, ZnSe film is soft and prone to deliquescence, and the residual stress of ZnS film is compressive stress [12], which can match the Ge film with tensile stress, and is beneficial to reduce the residual stress of the film. Therefore, ZnS is chosen as the middle refractive index material. The low refractive index material of LWIR band YbF<sub>3</sub> has a transparent area of 0.3~12 $\mu\text{m}$ , and a low refractive index is conducive to reducing the thickness of the film.

#### 4. Film design

According to the technical parameter requirements in Table 1, on the one hand, the passband half-width of narrow-band filter is about 70nm by increasing the number of passband reflection heap layers and the half-wave hierarchy, on the other hand, conventional film system is difficult to ensure the high penetration of 7.669  $\mu\text{m}$  while blocking the the 3~12 $\mu\text{m}$  band by widening the cut-off band.

In the process of film design, it is found when the number of optimized layers is less than 22, the secondary peak of the cut off region is difficult to be eliminated. At this time, the total physical thickness is 41.5 $\mu\text{m}$ , which is thick and requires high performance requirements on all aspects of the equipment. Moreover, the internal stress of the film layer deposited on one side is very large. According to the principle of split technology and the use of double-sided film system, the film is divided into two splits. The front surface film system is high transmission of  $7.669 \pm 0.035\mu\text{m}$ , cut off in 6.3~7.5 $\mu\text{m}$  and 7.8~9.8 $\mu\text{m}$ , and the back surface cut off in 3~6.3 $\mu\text{m}$  and 9.8~12 $\mu\text{m}$  band on the basis of high transmission of 7.669 $\mu\text{m}$ .

##### 4.1. Design of front surface

According to the spectral requirements of the front surface film system after splitting, in the initial

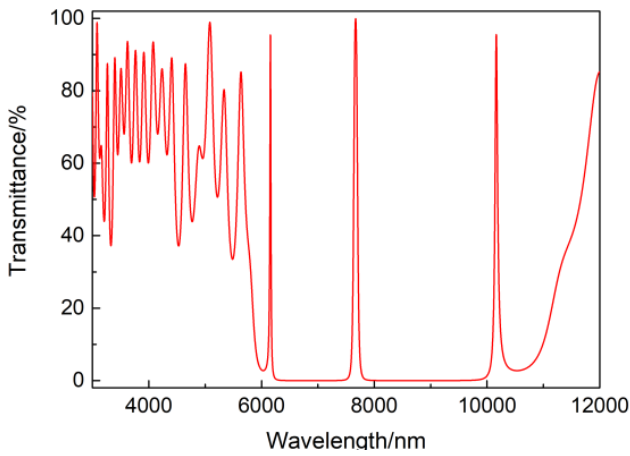
membrane system, the full-media double-half-wave narrow-band pass-through membrane system was adopted. The full-media Fabry-Perot filter has two kinds of structures whose half-wave interval layers are high refractive index materials and low refractive index materials respectively. Considering the characteristics of long-wave infrared materials and deposition process factors, a structure of low refractive index film as a resonant cavity, symmetrical distribution of reflective film on both sides is used. When the spacer layer is a low refractive index material, its passband half-width is:

$$2\Delta\lambda = \frac{4\lambda_0 n_L^{2x-1} n_s}{m\pi n_H^{2x}} \times \frac{(n_H - n_L)}{(n_H - n_L + n_L/m)} \quad (9)$$

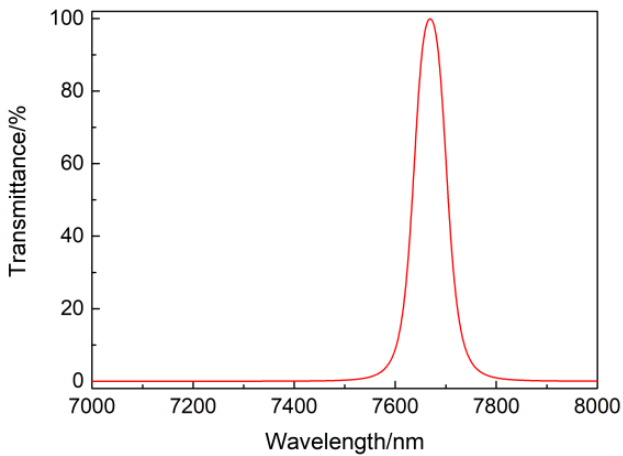
where  $2\Delta\lambda$  is the peak half-width of the narrow-band filter.  $n_H$ ,  $n_L$  represent the refractive index of the high and low refractive index materials.  $n_s$  represents a substrate of Ge,  $x$  is the number of high refractive index films in the reflective film,  $m$  is the resonant cavity level.

When the coating materials and the substrate are selected,  $n_H$ ,  $n_L$  and  $n_s$  are known amount.

According to the required passband half width to determine the interference level  $m$  and the reflective film within the high refractive index film number  $x$ . According to the film design theory, the base film system is Sub|HM<sub>1</sub>HM<sub>1</sub>HM<sub>2</sub>2M<sub>1</sub>HM<sub>1</sub>HM<sub>1</sub>M<sub>1</sub>HM<sub>1</sub>2M<sub>1</sub>HM<sub>1</sub>|Air, where Sub represents a substrate of Ge, H represents a high refractive index material Ge, M represents a medium refractive index material ZnS. The theoretical design spectral transmittance curve shown in Fig. 4. Without considering the case of back reflection, the transmittance of 7.669 $\mu\text{m}$  is 99.9%, the passband half width is 71nm, and the average transmittance of cut-off region 6.3 ~ 7.5 $\mu\text{m}$  and 7.8 ~ 9.8 $\mu\text{m}$  is 0.03%.



(a) 3~12μm



(b) 7~8μm

Fig. 4 Theory design spectral curve of front surface

4.2. Design of back surface

The back surface must meet the 3 ~ 6.3μm and 9.8 ~ 12μm band cut off, while the 7.62 ~ 7.82μm band has a high transmittance, in order to achieve narrow-band filter in the 7.669μm wavelength near the higher peak transmittance. Based on the principle of interference cut-off filter design, the initial film is Sub| 0.6(0.5HL0.5H)^4 (0.5HL0.5H)^4 2.7(0.5LH0.5L)^4 |Air, where Sub represents a substrate of Ge, H represents a high refractive index material Ge, L is the low refractive index material YbF<sub>3</sub>. The film system was optimized by Macleod software, and the optimized film system was Sub| 0.8871L 0.6552H 0.7875L 2.0496H

0.8399L 0.5255H 0.8392L 0.9116H 0.7795L 0.9400H  
 1.1562L 1.4168H 0.8096L 0.6937H 1.7576L 1.9680H  
 3.0138L 1.9092H 3.1568L 1.4571H 2.0248L 3.3577H  
 |Air. The physical thickness distribution of each film is shown in Fig. 5.

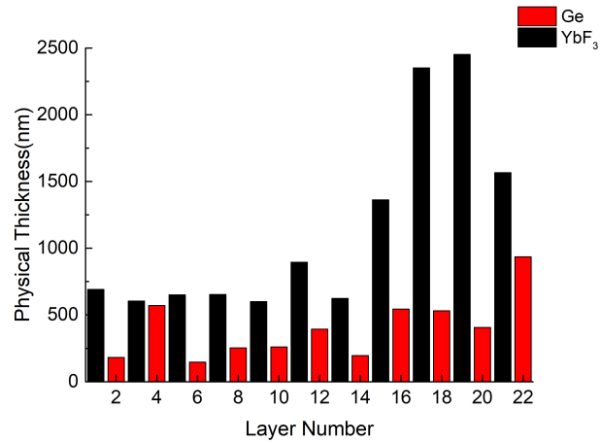


Fig. 5. Physical thickness distribution of back surface film

As is shown in Fig. 5, the thickness of the 17th and 19th layer are more than 2μm. According to the experiments, a single layer of YbF<sub>3</sub> is prone to crack if its thickness is more than 2μm [13] and residual stress of the YbF<sub>3</sub> film is tensile stress, and deposition with the Ge film will lead to a large residual stress and easily released. therefore, replacing the 17th and 19th layer with a compressive stress ZnS, which can effectively reduce the residual stress of the film, and optimizing it again to obtain the film system Sub| 0.9924L 0.5799H 0.7739L 2.1046H 0.8043L 0.3833H 1.0107L 0.9799H 0.6972L 0.9733H 1.2383L 1.3515H 0.8347L 0.7341H 16098L2.3751H 2.7624M17869H 3.0856M 1.5864H 2.0819L 3.4053H |Air, the film thickness distribution is shown in Fig. 6, and the theoretical design of the transmittance spectrum as shown in Fig.7. Without considering the back reflection, the average transmittance of 7.62~7.82μm is 99.98%, and the average transmittance of cut-off area 3 ~ 6.3μm and 9.8 ~ 12μm are 0.049% and 0.058%, respectively.

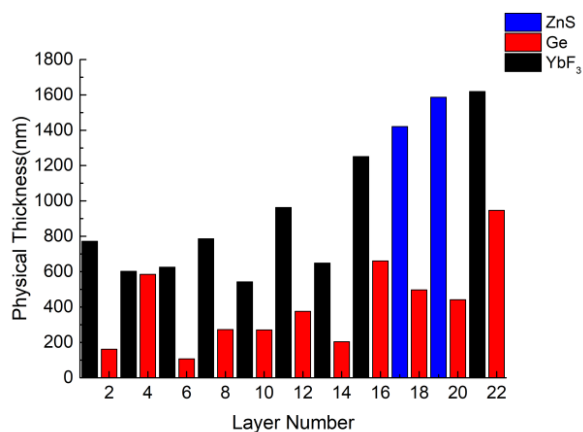


Fig. 6. Thickness distribution after adjustment

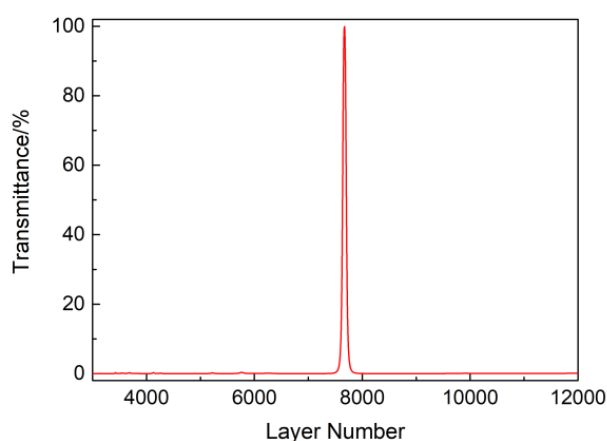


Fig. 8. Theory transmittance spectral curve of double-sided design

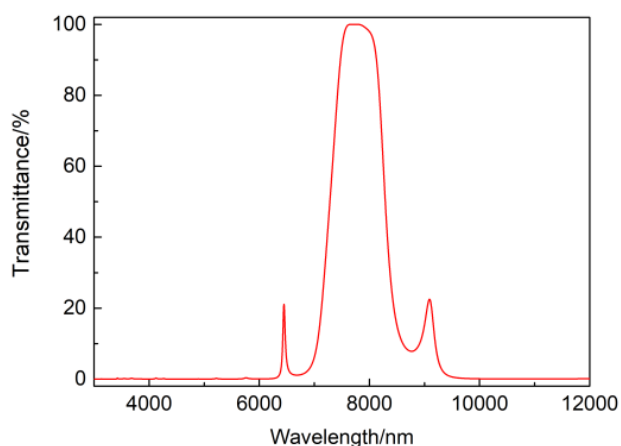


Fig. 7. Theory spectral curve of the back surface

### 4.3. Design of double-sides

The front and back surface film data were imported into the Macleod software, and the theoretical spectral transmittance curve of the narrowband filter was as shown in Fig. 8, the transmittance at 7.669 $\mu$ m was 99.9%, the average transmittance of cut-off region 3~7.5 $\mu$ m and 7.8 ~ 12 $\mu$ m was 0.04%.

## 5. Preparation of films

The experiment was performed on a Leybold Optics ARES1100 vacuum coating machine. It equipped with dual "e" electron guns, APS ion source, OMS 5000 optical film thickness monitoring system and six probe crystal control system.

### 5.1. Film preparation process parameters

Place the cleaned substrate on the rotate fixture of the vacuum chamber. When the vacuum reaches  $2 \times 10^{-3}$ pa, open the ion source bombarding of the substrate for 10 minutes, and deposit the films according to the process parameters in Table 2. After the deposition completed, take out and test when the vacuum chamber is cooled to room temperature.

Table 2. Process parameters

Material	Deposition rate /(nm/s)	Vacuum degree /Pa	Ratio of actual thickness to displayed thickness /%
Ge	0.25	$2.0 \times 10^{-3}$	91.9
ZnS	0.8	$2.0 \times 10^{-3}$	88.2
YbF <sub>3</sub>	0.5	$2.0 \times 10^{-3}$	82.8

**5.2. Film preparation monitoring method**

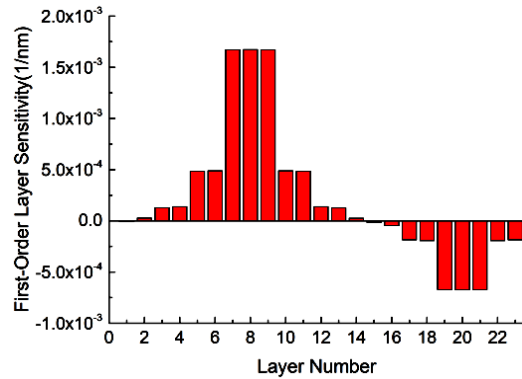
In order to obtain narrow-band filters with good optical properties, the film precision needs to be strictly controlled in the deposition process, otherwise a large cumulative error will occur, thus affecting the optical properties of the film. During the experiment, the quartz crystal monitoring method was used for monitoring [14]. The monitoring method is to measure the thickness of the film by monitoring the amount of change in the vibration frequency of the AT-cut quartz crystal. The working principle is

$$\Delta f = -\frac{\rho_M}{\rho_Q} \times \frac{f^2}{N} \Delta d_M \tag{10}$$

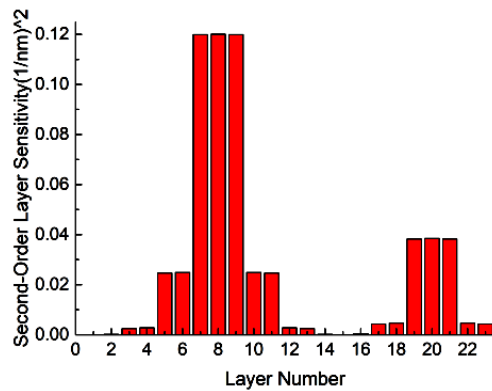
In formula (10),  $\Delta f$  is the change of crystal vibration frequency,  $\rho_M$  is the film density,  $f$  is the fundamental frequency of quartz crystal,  $\Delta d_M$  is the change of film thickness,  $\rho_Q$  is the density of quartz crystal,  $N$  is the frequency constant of quartz crystal. When the film material is given,  $\rho_M$  is known,  $-\left(\rho_M / \rho_Q\right) \cdot \left(f^2 / N\right)$  is usually a definite constant, The "-" indicates that the crystal vibration frequency decreases with the increase of the film thickness. As can be seen from equation (10), with the increase of film thickness, the vibration frequency of quartz crystal decreases continuously, and its monitoring sensitivity decreases correspondingly, thus resulting in slight errors. Film sensitivity is an evaluation function that measures the effect of film thickness error on the spectrum. The effect of this error on the insensitive film layer is not obvious. However, Minor errors can also affect the spectral characteristics for films with high sensitivity. Therefore, according to the distribution of film thickness and film sensitivity, reasonable

distribution of quartz crystal controller can play a great role in improving the spectral performance.

The sensitivity distribution of the film layer on the front surface is shown in Fig. 9.



(a) First-order sensitivity



(b) Second-order sensitivity

Fig. 9. Sensitivity distribution of surface film layer

It can be seen that the 7th, 8th, 9th, 19th, 20th and 21st layers are more sensitive. According to the sensitivity and thickness of the film, the monitoring mode is determined as shown in Fig. 10.

The sensitivity distribution of the surface film layer is shown in Fig. 11. It can be seen that the 2nd, 6th, 10th, 14th, 18th and 22th layers are more sensitive. Whenever the crystal control piece is dispensed, switch the new crystal piece as much as possible in these layers. Combined with the thickness distribution of the film layer, the monitoring mode is determined as shown in Fig. 12.

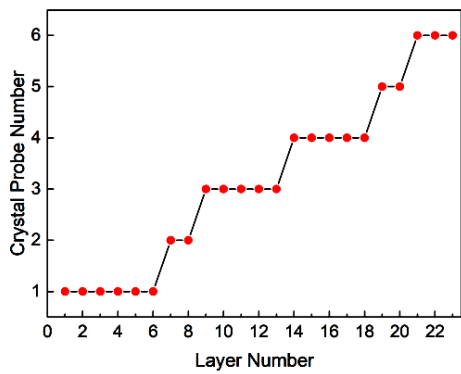
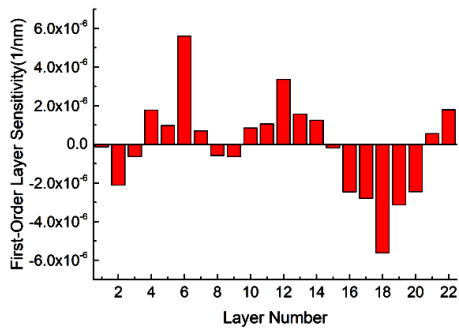
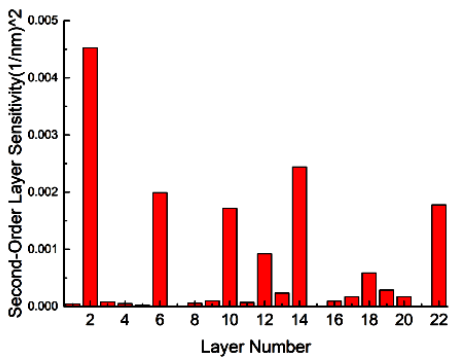


Fig. 10. Front Surface Crystal Control Distribution



(a) First-order sensitivity



(b) Second-order sensitivity

Fig. 11. Distribution of sensitivity of the back surface film

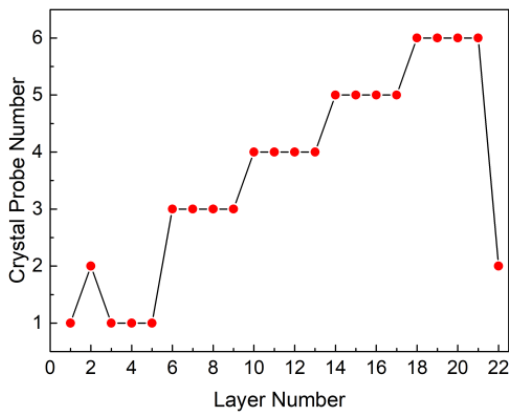
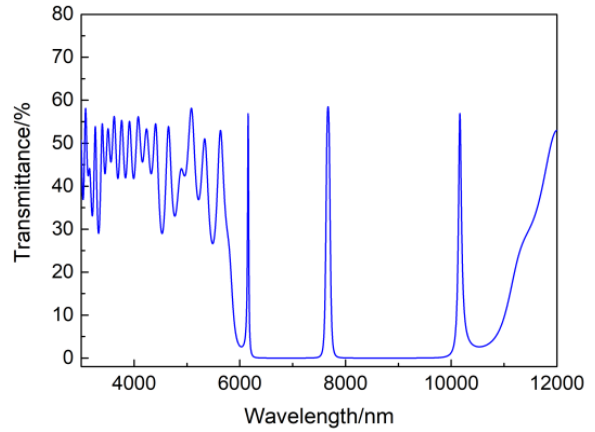


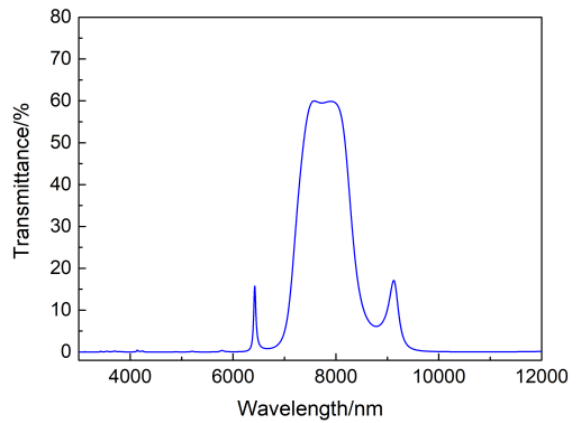
Fig. 12. Distribution of the rear surface crystal plate

6. Test results

The test sample transmittance was measured by a Varian660-IR Fourier transform infrared spectrometer manufactured by Varian.



(a) Front surface



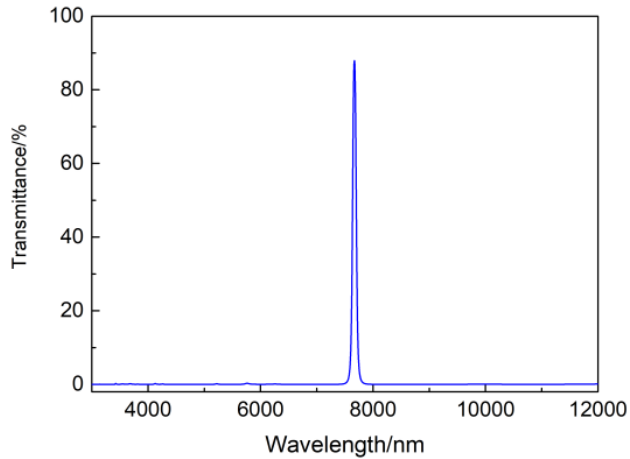
(b) Back surface

Fig. 13. Test transmission curves of single-sided coating

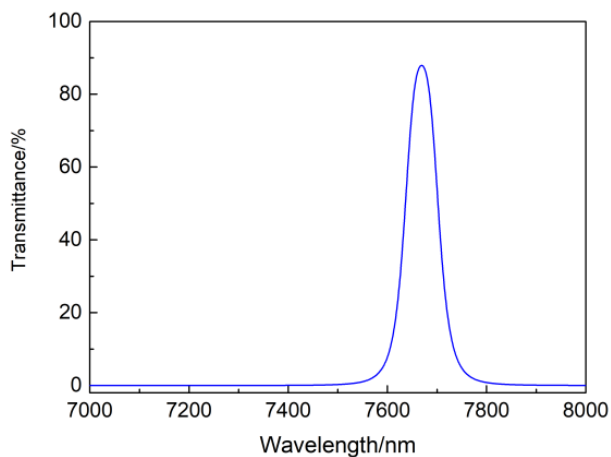
The test curve for single-sided coating transmittance was shown in Fig. 13. The peak transmittance of the single-side coating film on the front surface at the central wavelength at 7.669μm is 58.51%, and the average transmittance of cut-off area 6.3 ~ 7.5μm and 7.8 ~ 9.8μm is 0.116%. The average transmittance of the single-side coating film on the front surface of 7.62~7.82μm is 59.820%, and the average transmittance of cut-off area 3~6.5μm and 9.8~12μm is 0.132%.

The transmittance test curve for double-sided coating is shown in Fig. 14, the peak transmittance at 7.669μm is 87.88%, the peak half-width is 71nm, and the

average transmittance in the cut-off region  $3 \sim 7.5\mu\text{m}$  and  $7.8 \sim 12\mu\text{m}$  is 0.19%, which satisfies the technical specifications of spectroscopy.



(a)  $3\sim 12\mu\text{m}$



(b)  $7\sim 8\mu\text{m}$

Fig. 14. Test transmission curves of double-sided coating

To ensure the reliability of the performance of the narrowband filter, the sample is tested for firmness, adhesive tape with a viscosity of no less than 3N / cm was adhered to the surface of the film, ensuring smooth with no bubbles, and pulling the tape along the vertical direction of the film quickly. There is no phenomenon of stripping after repeating 20 times.

## 7. Conclusion

Based on the sensitivity of the methane gas infrared detection system and the difficulty coefficient of the narrow-band filter, a cost performance function is established. To obtain the technical parameters of the filter, the peak width of the narrowband filter is determined by calculating the extremum of the cost performance evaluation function and the control precision of the actual preparation and the sensitivity of the detection system in the actual application. Three kinds of materials Ge, ZnS and  $\text{YbF}_3$  were selected, and the double-sided design of the filter film was realized by software Macleod, using the principle of splitting technology and combining the thickness distribution of the film and the internal stress of the film. By analyzing the sensitivity of the membrane layer, the monitoring mode of the membrane layer can be adjusted reasonably so that the thickness of the sensitive layer of the membrane system can be controlled accurately. A narrow-band filter with a peak transmittance at  $7.669\mu\text{m}$  is 87.88%, a peak half width of 71 nm and a cut-off area of less than 0.19%, which can effectively suppress the background noise and improve the sensitivity of the detection system.

## Acknowledgments

This research was supported by a grant from the Major Scientific and Technological Projects of Jilin Province (No. 20140203002GX).

## References

- [1] A. Alvarez Ramón, Z. A. Daniel, D. R. Lyon et al., *Science* **6**(21), 7204 (2018).
- [2] Y. L. Li, A. L. Yao, Y. J. Li et al., *Natural Gas Industry* **24**, 102 (2004).
- [3] M. Du, D. F. Zhao et al., *Oil Gas S T*, (2012).
- [4] B. Zhang, G. Q. Chen et al., *China Population Resources & Environment* **22**(7), 8 (2012).
- [5] J. K. LI, W. Q. Jin et al., *J. B. Inst. Techno* **36**(6), 630 (2016).

- 
- [6] S. F. Xiong, X. H. Fu et al., *Acta Photonica Sinica* **46**(10), 80 (2017).
- [7] P. G. Wang et al., *Coatings* **8**(12), 472 (2018).
- [8] Y. Zhang, H. R. Wang et al., *Piezoelectrics and Acoustooptics* **2**, (2008).
- [9] S. W. Sun et al., *Chin. J. Lasers* **39**(07), 209 (2012).
- [10] H. Lin, C. L. Zhou, N. Zhao et al., *Laser and Optoelectronics Progress* **52**(12), 120102-1 (2015).
- [11] Y. F. Lu, X. Xiao, W. Q. Liu et al., *Chin. J. Lasers* **39**(B06), 14 (2012).
- [12] X. P. Song, *J. Funct. Mater.* **11**, 1734 (2006).
- [13] Y. D. Feng, T. Y. Yu, D. Q. Liu, *Acta Opt. Sin.* **38** (07), 385 (2018).
- [14] H. Yan, H. L. Hu, S. Q. Song et al., *Vacuum* **5**, 16 (2003).

---

\*Corresponding author: cc\_optics@163.com

xsf\_optics@126.com